Using six moments of Boltzmann's transport equation for device simulation

Tibor Grasser,[a] Hans Kosina, Markus Gritsch, and Siegfried Selberherr

Institute for Microelectronics, TU-Vienna, Gusshausstrasse 27–29, A-1040 Vienna, Austria

As has been frequently pointed out the distribution function of hot carriers in state-of-the-art devices is insufficiently described using just the average carrier energy. In this work the distribution function is characterized by six moments to obtain a more accurate description of hot carrier phenomena. A transport model based on six moments is derived and compared to a previously published model. A detailed comparison of results obtained from the model with Monte-Carlo data shows excellent agreement provided proper models for the relaxation times are used. © *2001 American Institute of Physics.* [DOI: 10.1063/1.1389757]

I. INTRODUCTION

For modern semiconductor devices nonlocal effects gain more and more importance. In the traditional drift-diffusion model the average carrier energy is assumed to be in equilibrium with the electric field. This assumption has been shown to be invalid as the average carrier energy lags behind the electric field because the carriers take some time to pick up energy from the electric field. In order to obtain information about this nonlocal behavior of the carrier energy, various hydrodynamic and energy-transport models have been proposed.[1,2] Furthermore, it was found that the average carrier energy provides a better basis for modeling parameters like mobility[3,4] and impact ionization[5,6] compared to approaches using the local electric field. In particular, the symmetric part of the distribution function is commonly modeled using a heated Maxwellian shape.[7] As has been frequently pointed out, this is at best a modest approximation in state-of-the-art devices where the gradients of the electric field are large. Two main deviations from the Maxwellian shape have been reported by many authors. First, it has been observed, that after a certain energy the slope of the distribution function decreases rapidly. This has been called the thermal tail of the distribution function because its effective temperature equals the lattice temperature. Abramo and Fiegna[8] discussed this thermal behavior of the high-energy tail which they proposed to appear for energies larger than $q \Delta \psi(x)$ with $\Delta \psi(x)$ being the voltage drop experienced by the carriers from the injecting contact up to the point x. They showed that this thermal behavior is not a band structure effect by reproducing it with a single isotropic and parabolic band, including only acoustic and optical phonon scattering. Furthermore, they showed that the effective temperature of the thermal tail is increased when electron–electron scattering (EES) is taken into account. The influence of EES has been investigated in detail by Chang *et al.*[9] who evaluated the influence of the band structure (parabolic versus fullband). Figure 5 in Ref. 9 indicates that the influence of the fullband structure is small and mainly influences the high-energy tail. Ghetti *et al.*[10] showed that the influence of EES on substrate and gate currents was negligible. In addition impact-ionization feedback was reported to change the thermal tail of the distribution function.[11,12]

Another important deviation from the Maxwellian shape occurs when hot and cold carrier populations mix, as is the case in the drain region of metal–oxide–semiconductor (MOS) transistors. These populations coexist for some time and can be described by a superposition of a hot and cold Maxwellian distribution.[13] In those regions, the relaxation times are largely determined by the average energy of the hot population. Since the number of hot carriers is frequently much smaller than the number of cold carriers the average energy of the hot carriers has only negligible influence on the energy of the whole electron gas and thus models using this energy are bound to fail.

Due to these deviations from the Maxwellian shape, the distribution function cannot be uniquely described by the average carrier energy. For the same average energies the distribution functions are completely different depending on whether they are taken from regions where the absolute value of the electric field increases or decreases.[14,15] As the relaxation times depend on the shape of the distribution function, problems are to be expected when they are modeled by using only the average carrier energy. In Ref. 15 the authors argue, that this might be the reason for the spurious velocity overshoots obtained by several energy-transport models[16,17] whereas Bordelon *et al.*[13] propose a solution to this problem by using two electron populations with two different temperatures.

II. HIGHER ORDER MOMENTS

To find a quantitative description of the deviation from the Maxwellian shape we look at the kurtosis β_ν of the distribution function which we define as

$$\beta_\nu = \frac{3}{5} \nu \frac{\langle \mathcal{E}^2 \rangle}{\langle \mathcal{E} \rangle^2} = \frac{4}{15} \frac{\langle \mathcal{E}^2 \rangle}{\nu \, k_B^2 \, T_\nu^2}. \tag{1}$$

In addition, we define a second order temperature Θ_ν as

$$\Theta_\nu = \beta_\nu T_\nu = \frac{2}{5 k_B} \frac{\langle \mathcal{E}^2 \rangle}{\langle \mathcal{E} \rangle} = \frac{4}{15} \frac{\langle \mathcal{E}^2 \rangle}{k_B^2 T_\nu}. \tag{2}$$

Here, ν denotes the carrier type (n or p), T_ν is the carrier temperature, $\mathcal{E}$ is the energy, and k_B is Boltzmann's constant. For a heated Maxwell–Boltzmann distribution and parabolic bands we get $\beta_\nu = \beta_{MB} = 1$ and therefore $\Theta_\nu = T_\nu$. Thus a $\beta_\nu \neq 1$ quantifies the deviation from the Maxwellian shape in the parabolic case. When nonparabolicity is taken into account, a different value for β_{MB} is obtained, which is close to 1 and temperature dependent. For instance, at 3000 and 6000 K, β_{MB} evaluates to 0.97 and 0.93, respectively.

As an example we considered an n^+–n–n^+ structure with the doping levels $N_D^+ = 10^{19}\,\mathrm{cm}^{-3}$ and $N_D = 10^{18}\,\mathrm{cm}^{-3}$ with a graded transition into a 0.3 μm long lowly doped region. This structure was simulated using a Monte-Carlo (MC) simulator employing optical and acoustic phonon scattering in addition to impurity scattering. Furthermore, nonparabolicity was considered using Kane's dispersion relation.[18] Both carrier temperatures, the kurtosis and typical distribution functions are shown in Fig. 1. Note that the average carrier energy at points A and D is equal whereas the distribution function looks completely different.[15] This can be clearly attributed to the kurtosis which is 0.8 at point A but 1.32 at point D. Furthermore, the shapes of the distribution functions for points A–C are similar, indicated by a similar value of β_n. In general it can be said that the distribution function is never anything like a Maxwellian, except for the contact regions. This clearly calls for a reinvestigation of the assumptions underlying the hydrodynamic transport models and the physical models used therein. Especially the relaxation times obtained from the relaxation time approximation are known to reflect a hysteresis when modeled as a function of the average energy only.[13,15,19]

In this article we propose a six moments (SM) model derived from Boltzmann's transport equation (BTE) which aims at modeling the kurtosis. We will also give a discretization and compare the results obtained by our model with the previously published six moments model by Sonoda *et al.*[20]

III. THE SIX MOMENTS MODEL

Several moment based models have been proposed which aim at obtaining some additional information about the distribution function to the average energy. One approach was to split the energy range at some characteristic energy and handle both energy ranges with a two-population and two-temperature model.[14,21] As these models were targeted on modeling impact ionization the band gap energy was taken as the characteristic energy. This approach leads to various additional parameters which model the transitions between the two energy regions. Determination of these parameters relies on carefully set up MC simulations. Due to this specialization to impact ionization, this model would have to be reformulated if another energy range is of interest as is the case for the calculation of gate currents.[22] Thus, this approach is difficult to generalize if both effects need to be captured at the same time which is the case for state-of-the-
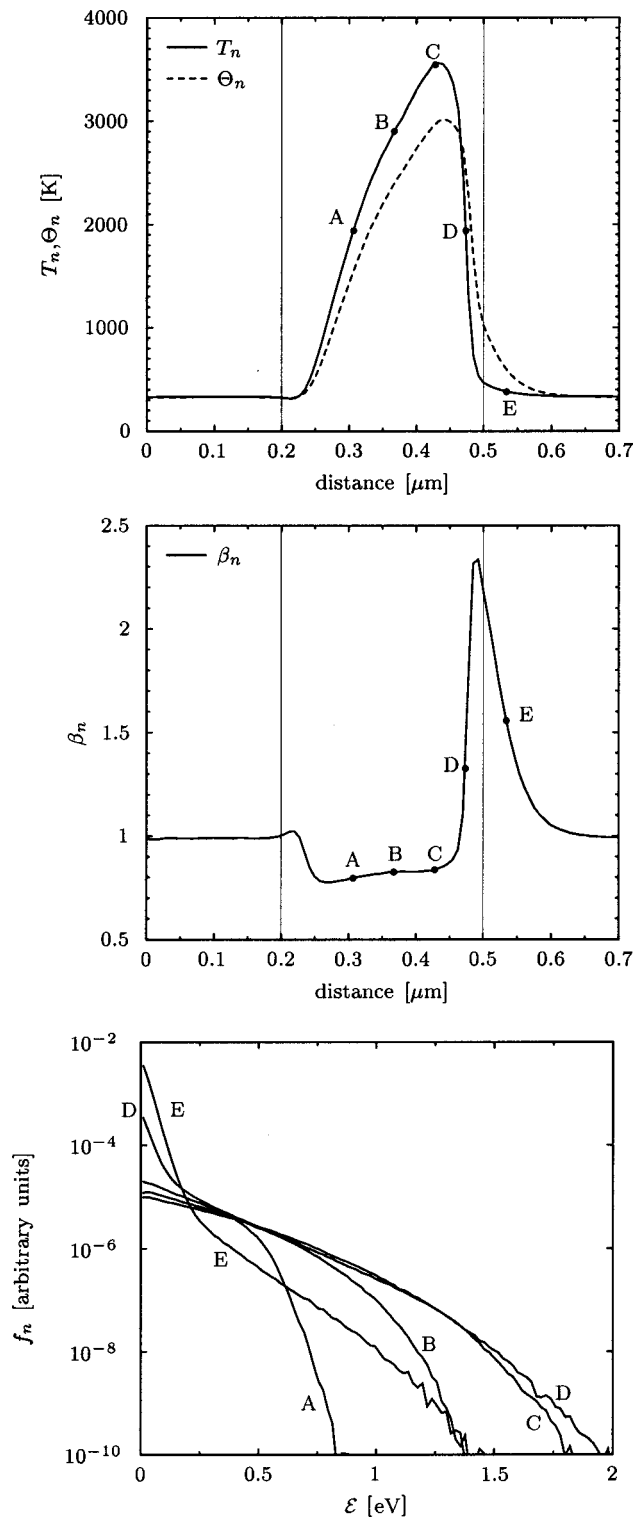

FIG. 1. Carrier temperature, absolute and relative kurtosis, and distribution functions at the five characteristics points of the n^+–n–n^+ structure. Note that the energies for A and D are the same.

art devices. A special formulation has been proposed in Ref. 13 for those regions where the high-energy tail is heavily populated $\beta_\nu > \beta_{MB}$. Unfortunately, this approach is limited to those regions and cannot capture effects in the regions with $\beta_\nu < \beta_{MB}$.

Several authors gave higher order moment equations to obtain additional accuracy; see e.g., Refs. 23 and 24. These

equations were based on an Ansatz for the distribution function which was taken to be some expansion around a Maxwellian shape. Sonoda *et al.*[20] added two equations for the fourth and fifth moment of the BTE to a standard energy-transport model taken from Ref. 25. This leaves the question open whether this results in a consistent equation set or not, an issue which will be addressed in the following where we derive a six moments model using the method of moments[26] without making any Ansatz for the distribution function. As with the derivation of the energy-transport model we start from Boltzmann's transport equation

$$\partial_t f + \mathbf{u} \cdot \nabla_{\mathbf{r}} f + s_\nu q \mathbf{E} \cdot \nabla_{\mathbf{p}} f = Q(f). \tag{3}$$

Here, q denotes the elementary charge, s_ν is the carrier charge (± 1), $\mathbf{E}$ is the electric field, $\mathbf{u}$ is the group velocity, and Q the collision operator. For the following we assume a single parabolic band with effective carrier mass m_ν. We use the following physically motivated weight functions instead of the powers of $\mathbf{k}$:

$$\Phi_0 = 1, \quad \Phi_1 = \mathbf{p} \quad = \hbar\, \mathbf{k},$$

$$\Phi_2 = \mathcal{E} = \frac{\hbar^2 \mathbf{k}^2}{2\, m_\nu}, \quad \Phi_3 = \mathbf{u}\, \mathcal{E},$$

$$\Phi_4 = \mathcal{E}^2, \quad \Phi_5 = \mathbf{u}\, \mathcal{E}^2,$$

$$\Phi_6 = \mathcal{E}^3,$$

and define the moments of the distribution function as

$$\hat{\mathrm{M}}_j = \langle \Phi_j \rangle = \int \Phi_j f\ d^3\mathbf{k}. \tag{4}$$

Taking the moments of Boltzmann's equation gives the following general moment equation:

$$\partial_t \langle \Phi_j \rangle + \nabla_{\mathbf{r}} \cdot \langle \mathbf{u} \otimes \Phi_j \rangle - s_\nu q \mathbf{E} \cdot \langle \nabla_{\mathbf{p}} \otimes \Phi_j \rangle$$

$$= \int \Phi_j\, Q(f)\, d^3\mathbf{k}, \tag{5}$$

where $\otimes$ denotes the tensor product[27] which reduces to the normal product for the scalar weight functions $(j = 0,2,4)$. The scattering integral is evaluated by employing the macroscopic relaxation time approximation

$$\int \Phi_j\, Q(f)\, d^3\mathbf{k} \cong -\frac{\langle \Phi \rangle - \langle \Phi \rangle_0}{\tau_\Phi}. \tag{6}$$

The term $\langle \nabla_{\mathbf{p}} \otimes \Phi_j \rangle$ evaluates for the first six moments as

$$\nabla_{\mathbf{p}} \Phi_0 = 0, \quad \nabla_{\mathbf{p}} \otimes \Phi_1 = \hat{\mathrm{I}}, \tag{7}$$

$$\nabla_{\mathbf{p}} \Phi_2 = \mathbf{u}, \quad \nabla_{\mathbf{p}} \otimes \Phi_3 = \frac{\mathcal{E}}{m_\nu} \hat{\mathrm{I}} + \mathbf{u} \otimes \mathbf{u}, \tag{8}$$

$$\nabla_{\mathbf{p}} \Phi_4 = 2\, \mathcal{E} \mathbf{u}, \quad \nabla_{\mathbf{p}} \otimes \Phi_5 = \frac{\mathcal{E}}{2} (\mathbf{u}^2 \hat{\mathrm{I}} + 4\, \mathbf{u} \otimes \mathbf{u}), \tag{9}$$

with $\hat{\mathrm{I}}$ being the unity tensor.

The assumptions made in the derivation of the moment equations follow consistently from appropriately scaling the BTE. The Knudsen number appears as scaling parameter, which represents the mean free path $\tau_0 v_0$ relative to the device dimension[28]

$$\lambda = \frac{\tau_0 v_0}{x_0}. \tag{10}$$

Here, τ_0 is the characteristic time between scattering events, v_0 denotes the velocity scale, and x_0 is given by the size of the simulation domain. Carriers in a semiconductor at room temperature can be considered a collision-dominated system, for which $\lambda \ll 1$. Diffusion scaling assumes the time scale of the system to be

$$t_0 = \frac{\tau_0}{\lambda^2}. \tag{11}$$

In the limit of vanishing Knudsen number, $\lambda \to 0$, one obtains that convective terms of the form $\langle \mathbf{u} \rangle \otimes \langle \mathbf{u} \rangle$ are neglected against $\langle \mathbf{u} \otimes \mathbf{u} \rangle$, one of the consequences being that the drift kinetic energy $m_\nu \langle \mathbf{u} \rangle^2 / 2$ is neglected against $k_B T_n$, and that in the flux equations the time derivative vanishes.

Knowing the outcome of diffusion scaling, we continue in this work from the unscaled BTE [Eq. (3)], split the distribution function into its symmetric and antisymmetric part, and apply the diffusion approximation, assuming that the symmetric part is isotropic, that is, it depends only on the modulus of $\mathbf{k}$:

$$f(\mathbf{k}) = f_S(|\mathbf{k}|) + f_A(\mathbf{k}). \tag{12}$$

This is the only assumption we need here to evaluate the tensor averages as

$$\langle \mathbf{u} \otimes \mathbf{u} \mathcal{E}^n \rangle = \frac{\langle \mathbf{u}^2 \mathcal{E}^n \rangle}{3} \hat{\mathrm{I}} = \frac{2}{3} \frac{\langle \mathcal{E}^{n+1} \rangle}{m_\nu} \hat{\mathrm{I}} \quad \text{with } n = 0,1,2. \tag{13}$$

Thus, we obtain the following balance equations where the subscript $\mathbf{r}$ has been dropped for the spatial Nabla operator:

$$\Phi_0: \quad \partial_t \langle 1 \rangle + \nabla \cdot \langle \mathbf{u} \rangle = 0, \tag{14}$$

$$\Phi_2: \quad \partial_t \langle \mathcal{E} \rangle + \nabla \cdot \langle \mathbf{u}\, \mathcal{E} \rangle - s_\nu q \mathbf{E} \cdot \langle \mathbf{u} \rangle = -\frac{\langle \mathcal{E} \rangle - \langle \mathcal{E} \rangle_0}{\tau_{\mathcal{E}}}, \tag{15}$$

$$\Phi_4: \quad \partial_t \langle \mathcal{E}^2 \rangle + \nabla \cdot \langle \mathbf{u}\, \mathcal{E}^2 \rangle - s_\nu 2\, q \mathbf{E} \cdot \langle \mathbf{u}\, \mathcal{E} \rangle$$

$$= -\frac{\langle \mathcal{E}^2 \rangle - \langle \mathcal{E}^2 \rangle_0}{\tau_\Theta}, \tag{16}$$

and the following flux equations:

$$\Phi_1: \quad \frac{2}{3} \nabla \langle \mathcal{E} \rangle - s_\nu q \mathbf{E} \langle 1 \rangle = -m_\nu \frac{\langle \mathbf{u} \rangle}{\tau_m}, \tag{17}$$

$$\Phi_3: \quad \frac{2}{3} \nabla \langle \mathcal{E}^2 \rangle - s_\nu \frac{5}{3} q \mathbf{E} \langle \mathcal{E} \rangle = -m_\nu \frac{\langle \mathbf{u}\, \mathcal{E} \rangle}{\tau_S}, \tag{18}$$

$$\Phi_5: \quad \frac{2}{3} \nabla \langle \mathcal{E}^3 \rangle - s_\nu \frac{7}{3} q \mathbf{E} \langle \mathcal{E}^2 \rangle = -m_\nu \frac{\langle \mathbf{u}\, \mathcal{E}^2 \rangle}{\tau_K}. \tag{19}$$

We now introduce new variables in analogy to the energy-transport model which gives the following densities and fluxes:

$$\Phi_0: \quad \langle 1 \rangle = \nu, \quad \Phi_1: \quad \langle \mathbf{u} \rangle = \frac{\mathbf{J}_\nu}{s_\nu q}, \quad (20)$$

$$\Phi_2: \quad \langle \mathcal{E} \rangle = \tfrac{3}{2} k_B \nu T_\nu, \quad \Phi_3: \quad \langle \mathbf{u}\mathcal{E} \rangle = \mathbf{S}_\nu, \quad (21)$$

$$\Phi_4: \quad \langle \mathcal{E}^2 \rangle = \frac{5 \times 3}{4} k_B^2 \nu T_\nu \Theta_\nu, \quad \Phi_5: \quad \langle \mathbf{u}\mathcal{E}^2 \rangle = \mathbf{K}_\nu, \quad (22)$$

$$\Phi_6: \quad \langle \mathcal{E}^3 \rangle = \frac{7 \times 5 \times 3}{8} k_B^3 \nu M_6. \quad (23)$$

The new variables are the second order temperature Θ_ν and the kurtosis flux $\mathbf{K}_\nu$. Furthermore, M_6 denotes the moment of sixth order which has to be modeled properly to close the equation system

$$\mathbf{J}_\nu = -C_1 \left[\nabla(\nu T_\nu) - s_\nu \frac{q}{k_B} \mathbf{E} \nu \right],$$

$$C_1 = s_\nu k_B \mu_\nu, \quad (24)$$

$$\mathbf{S}_\nu = -C_2 \left[\nabla(\nu T_\nu \Theta_\nu) - s_\nu \frac{q}{k_B} \mathbf{E} \nu T_\nu \right],$$

$$C_2 = \frac{5}{2} \frac{k_B^2}{q} \frac{\tau_S}{\tau_m} \mu_\nu, \quad (25)$$

$$\mathbf{K}_\nu = -C_3 \left[\nabla(\nu M_6) - s_\nu \frac{q}{k_B} \mathbf{E} \nu T_\nu \Theta_\nu \right],$$

$$C_3 = \frac{35}{4} \frac{k_B^3}{q} \frac{\tau_K}{\tau_m} \mu_\nu. \quad (26)$$

Here the mobility $\mu_\nu = q \tau_m / m_\nu$ is introduced. The balance equations read

$$\nabla \cdot \mathbf{J}_\nu = -s_\nu q (\partial_t \nu + R_\nu), \quad (27)$$

$$\nabla \cdot \mathbf{S}_\nu = -C_4 \partial_t(\nu T_\nu) + \mathbf{E} \cdot \mathbf{J}_\nu - C_4 \nu \frac{T_\nu - T_L}{\tau_\mathcal{E}} + G_{\mathcal{E}_\nu}, \quad (28)$$

$$\nabla \cdot \mathbf{K}_\nu = -C_5 \partial_t(\nu T_\nu \Theta_\nu) + 2 s_\nu q \mathbf{E} \cdot \mathbf{S}_\nu$$
$$- C_5 \nu \frac{T_\nu \Theta_\nu - T_L^2}{\tau_\Theta} + G_{\Theta_\nu}, \quad (29)$$

$$C_4 = \tfrac{3}{2} k_B \quad C_5 = \tfrac{15}{4} k_B^2. \quad (30)$$

Compared to energy-transport models, two additional relaxation times are needed, namely the relaxation time of the second order temperature τ_Θ, and the kurtosis flux relaxation time τ_K. Although the equation system could also be expressed in terms of β_ν instead of Θ_ν, the formulation with Θ_ν proved to be numerically more stable.

The boundary conditions assumed in the following simulations were of Dirichlet type for the contacts ($\nu = \nu^*$, $T_\nu = T_L$, and $\Theta_\nu = T_L$) and of Neumann type ($\mathbf{J}_\nu \cdot \mathbf{n} = 0$, $\mathbf{S}_\nu \cdot \mathbf{n} = 0$, and $\mathbf{K}_\nu \cdot \mathbf{n} = 0$) at the remaining boundaries.

Note that Eqs. (24), (25), (27), and (28) give a standard energy-transport model when Θ_ν is set equal to T_ν in Eq. (25).
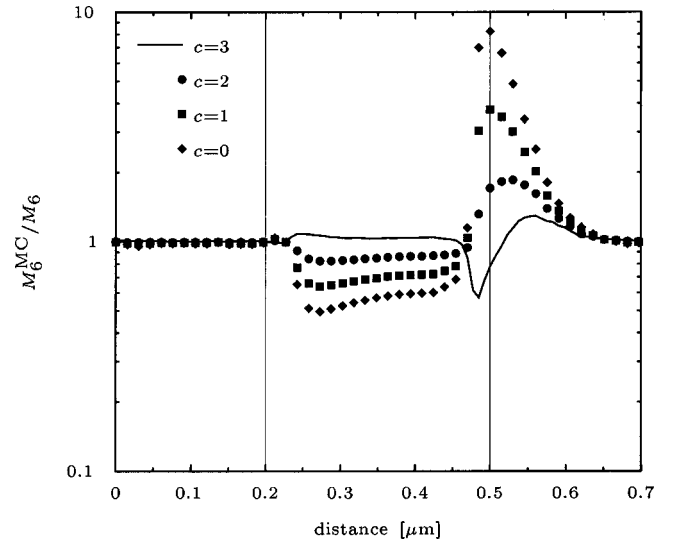

FIG. 2. Comparison of the different closure relations with the sixth moment from the MC simulation.

To close the equation system, the sixth moment M_6 still appearing in Eq. (26) has to be approximated using the lower order moments. From a Maxwellian distribution function and parabolic bands we know that $M_6 = T_\nu^3$. As we have the second order temperature Θ_ν available, we considered the following empirical closure relations:

$$M_6 = T_\nu^3 \left(\frac{\Theta_\nu}{T_\nu} \right)^c \quad \text{with} \quad c = 0, 1, 2, 3. \quad (31)$$

The ratio M_6^{MC}/M_6 is shown in Fig. 2. As can be seen, $c = 3$ gives the smallest deviation from the desired value, one. In addition $c = 3$ proved to be numerically more stable than other versions. Especially for $c = 1$, which corresponds to closing the system with a Maxwellian[20] the Newton procedure failed to converge in most cases.

Sonoda *et al.*[20] proposed a similar six moments transport model. One difference is that they used a microscopic relaxation time approximation as proposed by Stratton,[1] whereas in this work we assume the macroscopic relaxation time approximation (6). Sonoda *et al.* follow very closely the approach of Stratton, in that they assume a heated Maxwellian shape for the symmetric part of the distribution function. This assumption looks contradictory in that on one hand an additional moment of the distribution function is sought, and on the other hand, no additional degree of freedom is given to the distribution function. In this way, they introduce *two* closure relations, one for the fourth moment and one for the sixth moment. Therefore, their equation system gets decoupled into Stratton's energy transport model and an additional equation for the fourth moment. The role of the neglected coupling is elaborated in the example section where a detailed comparison with our model is given.

IV. DISCRETIZATION

For the discretization of the flux quantities we make use of the observation that all three fluxes $\mathbf{J}_\nu$, $\mathbf{S}_\nu$, and $\mathbf{K}_\nu$ can be written in a general form as

$$\mathbf{F} = -C_F \left[\nabla(\xi T_F) - s_\nu \frac{q}{k_B} E (\xi T_F) \frac{1}{T_F} \right] \quad (32)$$

with

$$\mathbf{J}_\nu: \quad \xi = \nu, \quad T_F = T_\nu, \tag{33}$$

$$\mathbf{S}_\nu: \quad \xi = \nu T_\nu, \quad T_F = \Theta_\nu, \tag{34}$$

$$\mathbf{K}_\nu: \quad \xi = \nu T_\nu \Theta_\nu, \quad T_F = \frac{\Theta_\nu^2}{T_\nu} = T_{\text{aux}}. \tag{35}$$

Assuming that the projected flux between two gridpoints is constant and that the temperature associated to each flux T_F varies linearly on the edge gives the following Scharfetter–Gummel type discretization[29] form of the flux

$$F_{i,j} = -\frac{C_F}{\Delta x} \frac{\Delta T_F}{\ln(T_{Fj}/T_{Fi})} [\xi_j \mathcal{B}(Y_F) - \xi_i \mathcal{B}(-Y_F)], \tag{36}$$

$$Y_F = -\frac{\ln(T_{Fj}/T_{Fi})}{\Delta T_F} \left(s_n \frac{q}{k_B} \Delta\psi + \Delta T_F \right), \tag{37}$$

where $\mathcal{B}$ is the Bernoulli function. The inner products $\mathbf{E} \cdot \mathbf{J}_\nu$ and $\mathbf{E} \cdot \mathbf{S}_\nu$ in Eqs. (28) and (29) are discretized in the following way. For any flux $\mathbf{F}$, the inner product can be written as

$$\mathbf{E} \cdot \mathbf{F} = -\nabla(\psi - \psi_{\text{ref}}) \cdot \mathbf{F} = -\nabla[(\psi - \psi_{\text{ref}})\mathbf{F}]$$
$$- (\psi - \psi_{\text{ref}}) \nabla \cdot \mathbf{F}. \tag{38}$$

Here an arbitrary constant offset in the potential is introduced, which, of course, does not change the electric field. Evaluating the inner product at grid point i using the local potential as reference ($\psi_{\text{ref}} = \psi_i$) gives

$$\mathbf{E} \cdot \mathbf{F}\big|_{\mathbf{x} = \mathbf{x}_i} = -\nabla[(\psi - \psi_i)\mathbf{F}] \tag{39}$$

which in turn is handled in a standard way by employing the box integration method.[30]

V. EXAMPLE AND DISCUSSION

To evaluate these six moments equations appropriate models for the relaxation times are needed. As expected, all relaxation times show a strong hysteresis when plotted over
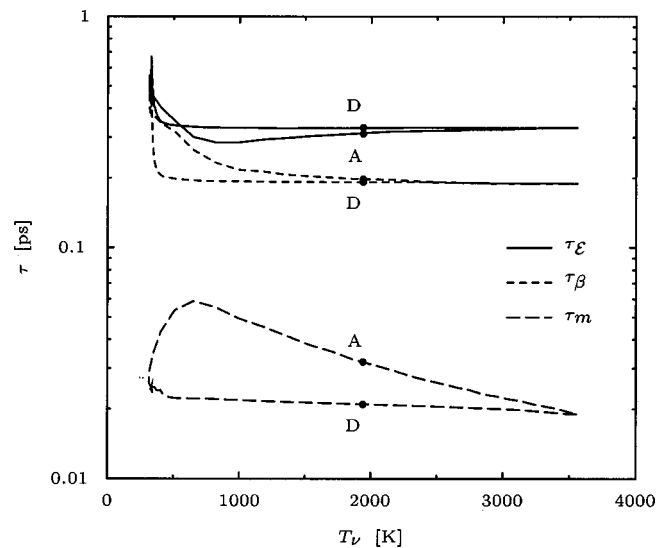

FIG. 3. Relaxation times as a function of the carrier temperature.

the average energy with the position as parameter (cf. Figs. 3 and 4). Nevertheless, in this article we assume for simplicity the following constant values $\tau_\mathcal{E} = 0.33$ ps, $\tau_\beta = 0.2$ ps, $\tau_S/\tau_m = 0.8$, and $\tau_K/\tau_m = 0.7$. More accurate expressions will be published elsewhere. The mobility is modeled using the MINIMOS mobility model.[31]

We now compare the results obtained by the SM model to MC simulations. Furthermore, we consider two simplified SM models obtained by assuming $\Theta_\nu = T_\nu$ in Eq. (25), which gives a decoupling of the equations as discussed before. For the simplified SM model SSM$_3$ we used the closure relation (31) with $c = 3$, as in the SM model, whereas in the model SSM$_1$ we used $c = 1$ which corresponds to the closure used by Sonoda *et al.* For the SSM models, the equation system is decoupled and consists of an energy-transport model and an additional constitutive equation for the second order temperature.
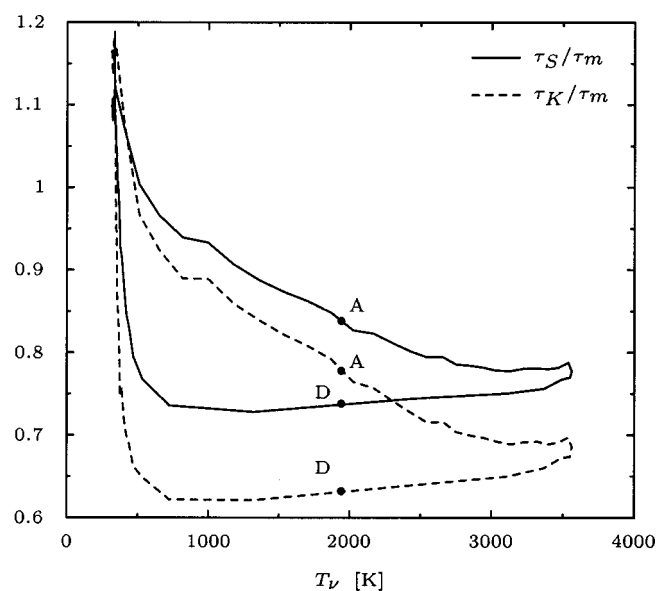

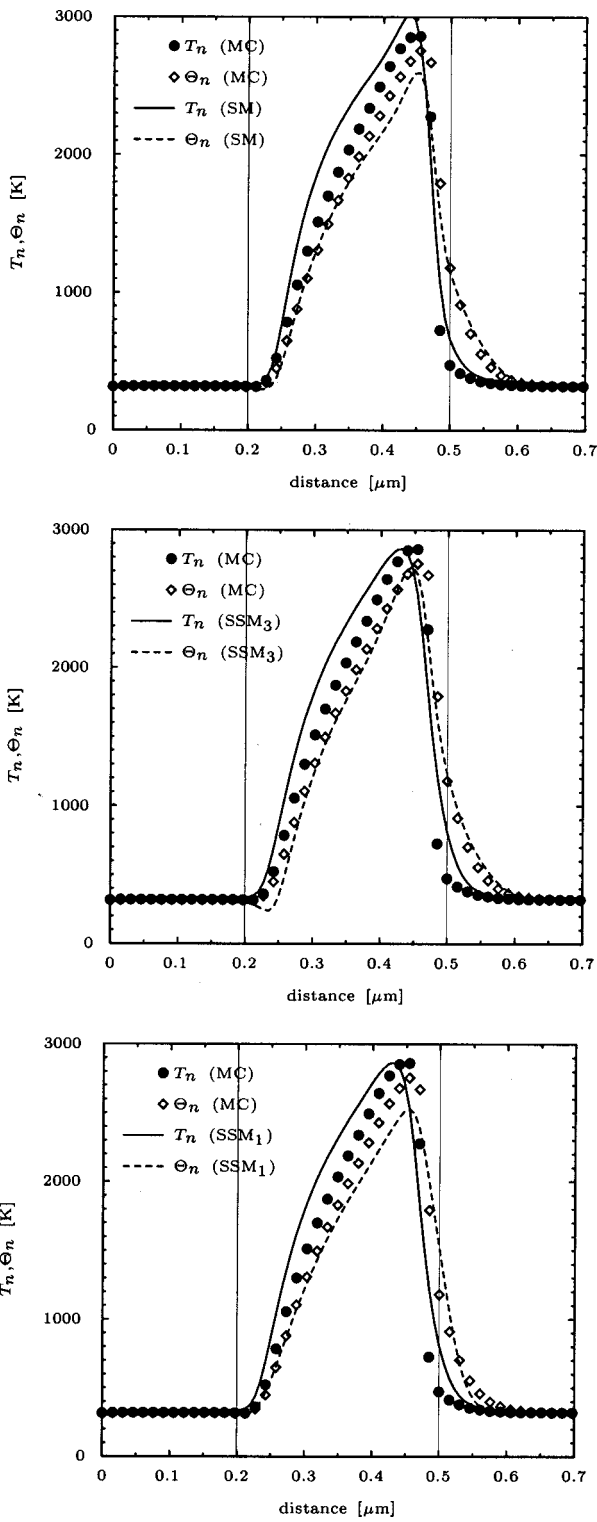FIG. 4. Relaxation times ratios as a function of the carrier temperature.

FIG. 5. Comparison of the results delivered by the SM, SSM_3, and the SSM_1 model with the parabolic MC results and constant relaxation times (excluding mobility).

FIG. 6. Comparison of the results delivered by the SM, SSM_3, and the SSM_1 model with the parabolic MC results and MC relaxation times (including mobility).

Simulation results of the n^+-n-n^+ structure are shown in Fig. 5. Since the moment equations are derived for parabolic bands we used a parabolic band structure in the MC simulations to allow for a fair comparison. The principal difference between the models is that due to the missing coupling term in the SSM models, the profile of the second o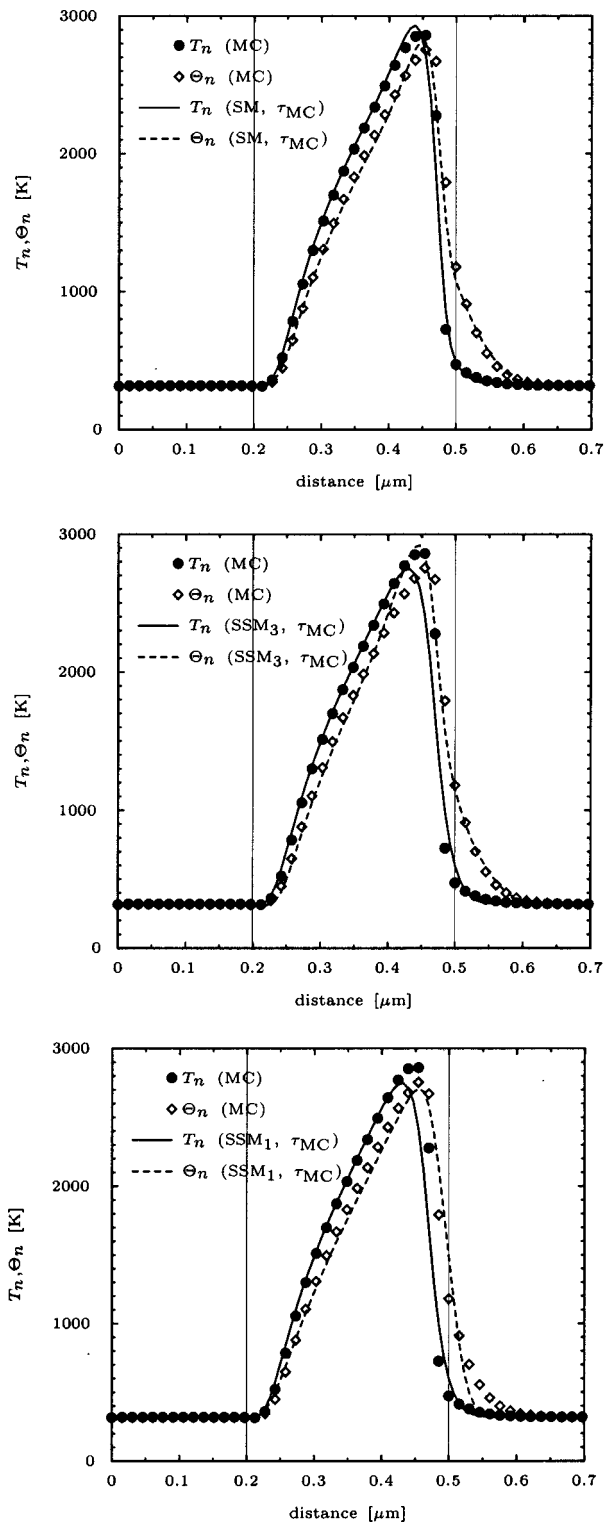rder temperature slightly drifts away from the temperature profile whereas in the SM model Θ_ν and T_ν stay tightly coupled. We observed an even stronger separation in the simulation of realistic MOS transistors. The SM model shows a better agreement with the MC simulations than the SSM models (cf. Fig. 5). For the moment equations constant relaxation times were used, except for the mobility which was calculated with the MINIMOS mobility model.[31] These
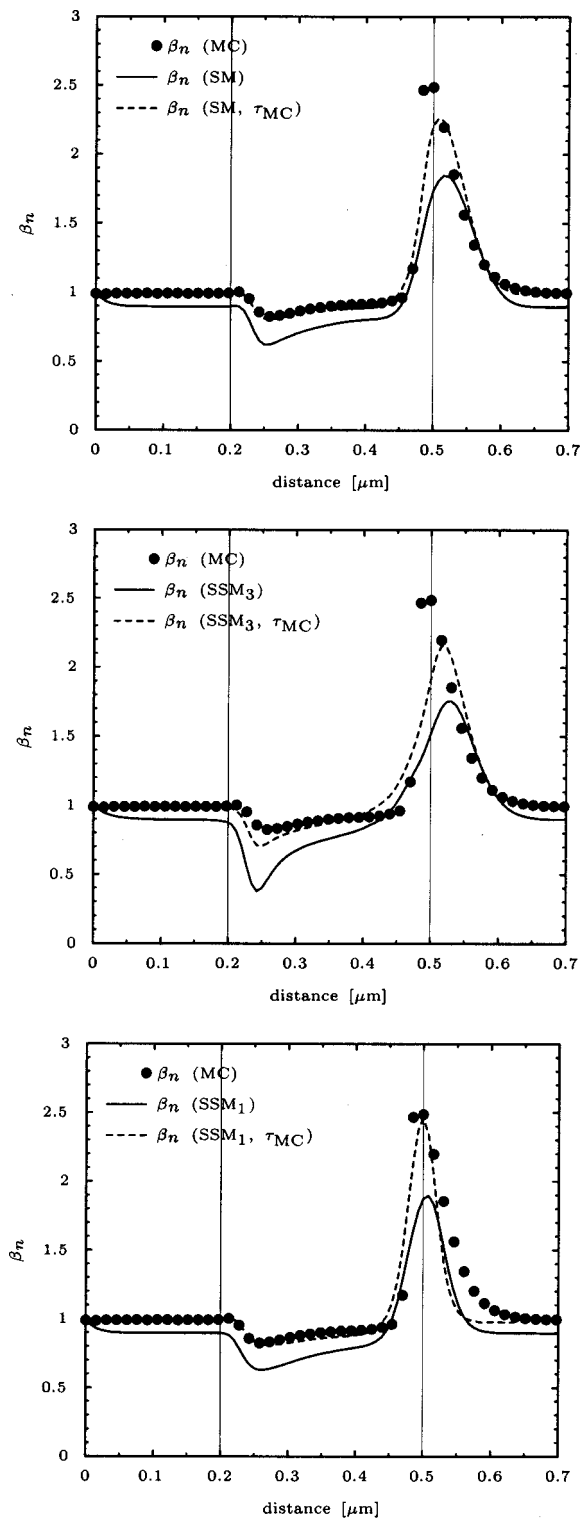
FIG. 7. Improvement of the accuracy by taking the MC relaxation times for the SM, SSM$_3$, and the SSM$_1$ model.

simulators were coupled to perform a self-consistent iteration where the potential distribution for the MC simulation was taken from the device simulator and the relaxation times for the device simulator from the last MC solution. Note that a large number of scattering events had to be processed to obtain smooth relaxation times with small variance. A comparison of simulation results is shown in Fig. 6 for the SM, SSM$_3$, and SSM$_1$ models, respectively. The SM very accurately conforms with the MC simulations whereas the decoupled models do not reach the maximum temperature values and start decreasing too early. The SSM$_3$ overestimates the second order temperature in the $n-n^+$ junction but fits the MC results quite well otherwise. On the other hand, the SSM$_1$ reproduces the maximum value of Θ_n while it decreases too sharply in the n^+ region. In Fig. 7 the kurtosis β_n is shown for all three models. Each subfigure shows the improvement due to the use of the MC relaxation times as compared with the constant relaxation times. Again, β_n decreases too rapidly in the n^+ region for the SSM$_1$ model. An obvious shortcoming of the constant relaxation times can be seen in the contact regions. There we would expect a Maxwellian distribution ($\beta_n=1$) which is not accurately reproduced by the constant relaxation times as their values have been taken from the high-energy regions. To improve the accuracy of the model, the relaxation times need to be modeled more carefully which will be the subject of forthcoming research.

VI. CONCLUSIONS

It has been frequently pointed out that the distribution function of carriers in state-of-the-art devices is insufficiently described by a Maxwellian distribution, which has the mean energy as only parameter. In this work we propose the usage of six moments of the distribution function, to allow for a more accurate description of hot-electron phenomena. Six moment equations are derived from the Boltzmann equation, and different closure relations are investigated.

To eliminate the uncertainties introduced by the relaxation time models we extracted the relaxation times from a Monte-Carlo simulator which was coupled to the six moments model in a self-consistent manner. This comparison showed an excellent agreement of the six moments model with the MC results.

ACKNOWLEDGMENTS

constant relaxation times were approximated using the data in Figs. 3 and 4, but no fitting for any of the models was performed. The results show the correct tendency, but there is still some discrepancy.

To estimate the influence of the relaxation times, we directly used the relaxation times obtained from the MC simulation, including the mobility. To do this, the device and MC

[1] R. Stratton, Phys. Rev. **126**, 2002 (1962).
[2] K. Bløtekjær, IEEE Trans. Electron Devices **ED−17**, 38 (1970).
[3] W. Hänsch, *The Drift Diffusion Equation and its Application in MOSFET Modeling* (Springer, New York, 1991).
[4] G. Baccarani and M. Wordeman, Solid-State Electron. **28**, 407 (1985).
[5] W. Quade, E. Schöll, and M. Rudan, Solid-State Electron. **36**, 1493 (1993).
[6] K. Souissi *et al.*, IEEE Trans. Electron Devices **40**, 1501 (1993).
[7] M. Lundstrom, *Fundamentals of Carrier Transport*, Modular Series on Solid State Device, Vol. X (Addison-Wesley, Reading, MA, 1990).
[8] A. Abramo and C. Fiegna, J. Appl. Phys. **80**, 889 (1996).

[9] M. Chang, D. Dyke, C. Leung, and P. Childs, J. Appl. Phys. **82**, 2974 (1997).

[10] A. Ghetti, L. Selmi, R. Bez, and E. Sangiorgi, International Electron Devices Meeting, 1996, pp. 379–382.

[11] J. Bude, IEEE Symposium on VLSI Technology Digest of Technical Papers 101, 1995.

[12] C. Jungemann, S. Yamaguchi, and H. Goto, in *27th European Solid-State Device Research Conference*, edited by H. Grünbacher (Editions Frontieres, Stuttgart, 1997), pp. 336–339.

[13] T. Bordelon *et al.*, Electron. Lett. **28**, 1173 (1992).

[14] P. Scrobohaci and T.-W. Tang, IEEE Trans. Electron Devices **41**, 1197 (1994).

[15] G. Wolokin and J. Frey, in Proceedings of NASECODE VIII, Vienna, 1992, pp. 107–108.

[16] Y. Apanovich *et al.*, IEEE Trans. Comput.-Aided Des. **13**, 702 (1994).

[17] D. Chen *et al.*, International Workshop on Numerical Modeling of Processes and Devices for Integrated Circuits NUPAD IV, Seattle, Washington, 1992, pp. 109–114.

[18] E. Kane, J. Phys. Chem. Solids **1**, 249 (1957).

[19] S.-C. Lee and T.-W. Tang, Solid-State Electron. **35**, 561 (1992).

[20] K. Sonoda, M. Yamaji, K. Taniguchi, C. Hamaguchi, and S. T. Dunham, J. Appl. Phys. **80**, 5444 (1996).

[21] J.-G. Ahn *et al.*, IEEE Electron Device Lett. **15**, 348 (1994).

[22] K. Hasnat *et al.*, IEEE Trans. Electron Devices **44**, 129 (1997).

[23] B. Geurts, M. Nekovee, H. Boots, and M. F. H. Schuurmans, Appl. Phys. Lett. **59**, 1743 (1991).

[24] S. Liotta and H. Struchtrup, Solid-State Electron. **44**, 95 (2000).

[25] M. Vecchi and L. Reyna, Solid-State Electron. **37**, 1705 (1994).

[26] M. Rudan, A. Gnudi, and W. Quade, in *Process and Device Modeling for Microelectronics*, edited by G. Baccarani (Elsevier, Amsterdam, 1993), pp. 109–154.

[27] E. Azoff, Solid-State Electron. **30**, 913 (1987).

[28] C. Ringhofer, C. Schmeiser, and A. Zwirchmayer, SIAM (Soc. Ind. Appl. Math.) J. Numer. Anal. (to be published).

[29] T.-W. Tang, IEEE Trans. Electron Devices **ED-31**, 1912 (1984).

[30] S. Selberherr, *Analysis and Simulation of Semiconductor Devices* (Springer, New York, 1984).

[31] S. Selberherr, W. Hänsch, M. Seavey, and J. Slotboom, Solid-State Electron. **33**, 1425 (1990).